Contribution from the Department of Chemistry,
University of Houston, Houston, Texas 77204-5641

Influence of Trans Axial Ligands on Five-Coordinate σ-Bonded Metalloporphyrins. Structural, Electrochemical, and Spectral Investigations of (OEP)Ir(C_3H_7)(L) Complexes

K. M. Kadish,* J.-L. Cornillon, P. Mitaine, Y. J. Deng, and J. D. Korp

Received October 17, 1988

The ligand-binding reactions of (OEP)Ir(C_3H_7) with triethylamine, pyridine, *N*-methylimidazole, dimethyl sulfoxide, triphenylphosphine, triethyl phosphite, and carbon monoxide were monitored by UV-visible and ^1H NMR spectroscopy, electrochemistry, and spectroelectrochemistry. Formation constants for addition of the sixth axial ligand, L, to (OEP)Ir(C_3H_7) ranged between $10^{1.6}$ and $10^{8.2}$, depending upon the nature of the specific ligand. (OEP)Ir(C_3H_7) and (OEP)Ir(C_3H_7)(L), where L = pyridine, *N*-methylimidazole, Me_2SO, and CO, could be oxidized by one electron without cleavage of the Ir-carbon bond on the cyclic voltammetry time scale. However, a fast chemical reaction followed the first electron abstraction from (OEP)Ir(C_3H_7)(L) when L was PPh_3 or $P(OEt)_3$, and [(OEP)Ir(PPh_3)]$^+ClO_4^-$ or [(OEP)Ir($P(OEt)_3$)]$^+ClO_4^-$ was obtained as the final oxidation product. The influence of the σ- and π-bonding properties of the ligand, L, on the ^1H NMR spectra, electronic absorption spectra, and electrochemistry of (OEP)Ir(C_3H_7)(L) is discussed, and the X-ray crystal structures of (OEP)Ir(C_3H_7)(PPh_3) (**1**) and (OEP)Ir(C_3H_7)(Me_2SO) (**2**) are presented. Compound **1** crystallizes as the perdeuterated benzene solvate in the triclinic system, space group $P\bar{1}$, with cell constants a = 14.105 (7) Å, b = 14.098 (7) Å, c = 14.032 (8) Å, α = 89.20 (4)°, β = 102.76 (4)°, γ = 89.63 (4)°, and Z = 2. The final R value is 0.038, and the Ir-C and Ir-P bond lengths are 2.063 (6) and 2.537 (1) Å, respectively. Compound **2** is triclinic, space group $P\bar{1}$, with a = 11.040 (5) Å, b = 11.179 (5) Å, c = 15.689 (7) Å, α = 95.58 (3)°, β = 90.71 (3)°, γ = 99.79 (3)°, and Z = 2. The final R value is 0.047 with Ir-C = 2.08 (1) Å and Ir-S = 2.436 (3) Å.

Introduction

The synthesis and characterization of metalloporphyrins with metal-carbon[1-4] or metal-metal[5-8] bonds have received increasing attention over the last few years.[9-11] Iron and cobalt alkyl or aryl σ-bonded porphyrins are of considerable interest for understanding the function and reactivity of several biological macromolecules.[3,12,13] σ-Bonded alkyl- and arylporphyrins are also good precursors in the synthesis of bi- or trimetallic metal-metal-bonded porphyrins,[1,7,11,14] and in this regard, a number of different main-group and transition-metal complexes have now been synthesized.[5,15,16]

The syntheses of σ-bonded porphyrins of the type (P)Ir(R), where P is the dianion of a given porphyrin ring and R is an alkyl or aryl group, have been known for almost 10 years,[17-19] but very few studies have been carried out on different types of (P)Ir(R) complexes. Only one paper has been published on the trans axial ligand effects of (P)Ir(R)(L),[18] and no detailed study involving the ligand-addition reactions of (P)Ir(R) or the spectroelectrochemistry of (P)Ir(R)(L) has ever been published. There is also no X-ray structure of a six-coordinate σ-bonded Ir porphyrin in the literature. The present study provides such information and presents the ligand-binding and ligand-exchange reactions of (OEP)Ir(C_3H_7) and (OEP)Ir(C_3H_7)(L).

Each ligand-addition and ligand-exchange reaction was monitored or characterized by UV-visible spectroscopy, ^1H NMR spectroscopy, electrochemistry, and spectroelectrochemistry. Both the spectral and the electrochemical behavior of the six-coordinate complex are dramatically affected by the nature of the sixth axial ligand (L). This is discussed in terms of the bonding properties of the ligands to (OEP)Ir(C_3H_7). In order to have a better understanding of the influence of an axial ligand on the Ir-carbon porphyrin complex, X-ray structures of (OEP)Ir(C_3H_7)(PPh_3) and (OEP)Ir(C_3H_7)(Me_2SO) are also presented.

Experimental Section

Chemicals. Methylene chloride (CH_2Cl_2, HPLC grade) was purified by double distillation over CaH_2. Tetrahydrofuran (THF, HPLC grade) was purified by distillation from Na-benzophenone. Benzonitrile was distilled under vacuum from P_2O_5. Triethylamine (NEt_3), pyridine (py), *N*-methylimidazole (N-MeIm), dimethyl sulfoxide (Me_2SO), triphenylphosphine (PPh_3), and triethyl phosphite ($P(OEt)_3$) were purified according to literature procedures and stored under argon. All solvents were distilled under an argon atmosphere prior to use. Tetrabutylammonium perchlorate ((TBA)ClO_4) was twice recrystallized from absolute ethanol, dried under vacuum, and stored in a vacuum oven at 40 °C. Argon (oxygen-free grade), high-purity carbon monoxide, and a 10% carbon monoxide-90% argon mixture were purchased from IWECO and Matheson.

(OEP)Ir(C_3H_7) was synthesized from (OEP)Ir(CO)Cl[17] according to the following two synthetic routes.

Method 1. Na/Hg Reduction. A 1% Na amalgam in THF was slowly added to 30 mg of (OEP)Ir(CO)Cl dissolved in 20 mL of THF. The reduction was monitored by UV-visible spectroscopy. After the characteristic UV-visible spectrum of (OEP)Ir(CO)Cl disappeared, the solution was cooled to -77 °C and an excess of $CH_3(CH_2)_2I$ was slowly added to the solution. The solution was then stirred for 30 min, warmed to room temperature, and stirred for another 30 min. THF was vacu-

(1) Guilard, R.; Kadish, K. M. *Chem. Rev.* **1988**, *88*, 1121-1146.
(2) Collman, J. P.; Brauman, J. I.; Madonik, A. M. *Organometallics* **1986**, *5*, 310.
(3) Callot, H. J.; Metz, F. *J. Chem. Soc., Chem. Commun.* **1982**, 947.
(4) Wayland, B. B.; Woods, B. A. *J. Chem. Soc., Chem. Commun.* **1981**, 700.
(5) (a) Cocolios, P.; Chang, D.; Vittori, O.; Guilard, R.; Moise, C.; Kadish, K. M. *J. Am. Chem. Soc.* **1984**, *106*, 5724. (b) Guilard, R.; Mitaine, P.; Moïse, C.; Lecomte, C.; Boukhris, A.; Swistak, C.; Tabard, A.; Lacombe, D.; Cornillon, J.-L.; Kadish, K. M. *Inorg. Chem.* **1987**, *26*, 2467. (c) Guilard, R.; Zrineh, A.; Ferhat, M.; Tabard, A.; Mitaine, P.; Swistak, C.; Richard, P.; Lecomte, C.; Kadish, K. M. *Inorg. Chem.* **1988**, *27*, 697.
(6) Onaka, S.; Kondo, Y.; Yamashita, M.; Tatematsu, Y.; Kato, Y.; Goto, M.; Ito, T. *Inorg. Chem.* **1985**, *24*, 1070.
(7) Kadish, K. M.; Guilard, R. *Comments Inorg. Chem.* **1988**, *7*, 287.
(8) Collman, J. P.; Barnes, C. E.; Swepston, P. N.; Ibers, J. A. *J. Am. Chem. Soc.* **1984**, *104*, 3500.
(9) Kadish, K. M. *Prog. Inorg. Chem.* **1986**, *34*, 435-605.
(10) Brothers, P. J.; Collman, J. P. *Acc. Chem. Res.* **1986**, *19*, 209.
(11) Guilard, R.; Lecomte, C.; Kadish, K. M. *Struct. Bonding* **1987**, *64*, 205-268.
(12) Mansuy, D.; Battioni, J. P. *J. Chem. Soc., Chem. Commun.* **1982**, 638.
(13) Brault, D.; Bizet, C.; Morliere, P.; Rougee, M.; Land, E. J.; Santus, R.; Shallow, A. J. *J. Am. Chem. Soc.* **1980**, *102*, 1015.
(14) (a) Cocolios, P.; Moïse, C.; Guilard, R. *J. Organomet. Chem.* **1982**, *228*, C43. (b) Guilard, R.; Mitaine, P.; Moïse, C.; Cocolios, P.; Kadish, K. M. *New J. Chem.* **1988**, *12*, 699.
(15) Coutsolelos, A.; Guilard, R. *J. Organomet. Chem.* **1983**, *253*, 273.
(16) (a) Kadish, K. M.; Boisselier-Cocolios, B.; Cocolios, P.; Guilard, R. *Inorg. Chem.* **1985**, *24*, 2139. (b) Kadish, K. M.; Boisselier-Cocolios, B.; Coutsolelos, A.; Mitaine, P.; Guilard, R. *Inorg. Chem.* **1985**, *24*, 4521. (c) Tabard, A.; Guilard, R.; Kadish, K. M. *Inorg. Chem.* **1986**, *25*, 4277. (d) Tabard, A.; Zrineh, A.; Guilard, R.; Kadish, K. M. *Inorg. Chem.* **1987**, *26*, 2459.
(17) Ogoshi, H.; Setsune, J.; Yoshida, Z. *J. Organomet. Chem.* **1978**, *159*, 317.
(18) Sugimoto, H.; Ueda, N.; Mori, M. *J. Chem. Soc., Dalton Trans.* **1982**, 1611.
(19) Cornillon, J.-L.; Anderson, J. E.; Swistak, C.; Kadish, K. M. *J. Am. Chem. Soc.* **1986**, *108*, 7633.

0020-1669/89/1328-2534$01.50/0

um-distilled, and the solid was purified by chromatography (silica gel–benzene).

Method 2. Electrochemical Reduction. A 20-mg sample of (OEP)Ir(CO)Cl in 15 mL of THF containing 0.1 M (TBA)ClO_4 was electrolyzed at −1.6 V vs SCE in an H-cell connected to a vacuum line. The reduction was assumed to be complete after the current decayed to about 5% of its starting value. The solution of $[(OEP)Ir]^-$ was cooled to −77 °C and transferred via a cannula to a THF solution containing an excess of $CH_3(CH_2)_2I$ at −77 °C. The same workup procedure was followed as above. After removal of (TBA)ClO_4 by filtration in benzene, the filtrate was chromatographed on silica gel. The crude solid was then recrystallized from a mixture of benzene and hexane. These two procedures yielded (OEP)Ir(C_3H_7) in yields ranging from 60% to 80%. The purity of the product was checked by ^1H NMR and UV–visible spectroscopy and electrochemistry.

Synthesis of (OEP)Ir(C_3H_7)(PPh_3). To a solution of (OEP)Ir(C_3H_7) (30 mg) in benzene (10 mL) was added 2 equiv of PPh_3. The solution was then allowed to evaporate slowly at room temperature for 2 weeks, and crystals of (OEP)Ir(C_3H_7)(PPh_3) suitable for X-ray diffraction were obtained.

Synthesis of (OEP)Ir(C_3H_7)(Me_2SO). To a solution of (OEP)Ir(C_3H_7) (30 mg) in benzene (10 mL) was added 2 equiv of Me_2SO. The solution was then allowed to evaporate slowly at room temperature for 5 weeks, and crystals of (OEP)Ir(C_3H_7)(Me_2SO) suitable for X-ray diffraction were obtained.

Instrumentation. Cyclic voltammetry was performed with the use of a conventional three-electrode system. The working electrode was a gold button (A = 0.85 mm^2). A commercial saturated calomel electrode was generally used as the reference electrode, but in some cases a silver-wire pseudo reference electrode was used. The reference electrode, in both cases, was separated from the bulk solution by a fritted-glass bridge, which contained the nonaqueous solvent and the supporting electrolyte. Potentials were referenced to the ferrocene/ferrocenium (Fc/Fc^+) couple when the silver-wire pseudo reference electrode was used. An IBM EC 225 voltammetric analyzer, an EG&G Model 175 universal programmer, or a BAS 100 electrochemical analyzer was used for cyclic voltammetry experiments. Controlled-potential electrolysis was performed with an EG&G Model 173 potentiostat. Both the reference electrode and the platinum-grid counter electrode were separated from the bulk solution by a fritted-glass bridge.

Unless otherwise noted, the supporting electrolyte was 0.1 M (TBA)ClO_4 for all electrochemical experiments. The sample concentration for electrochemistry ranged between 1.3×10^{-3} and 2.0×10^{-3} M. Thin-layer spectroelectrochemical measurements were performed with an IBM EC 225 voltammetric analyzer or an EG&G Model 173 potentiostat coupled with a Tracor Northern 1710 holographic optical spectrometer/multichannel analyzer. The construction and properties of the optically transparent thin-layer electrode have been described in the literature.[20]

Titrations of (OEP)Ir(C_3H_7) and (OEP)Ir(C_3H_7)(L) with carbon monoxide were performed with a Matheson Model 8250 modular Dyna-blender. The gas flow meters of this system allowed for argon–carbon monoxide mixtures of known concentration to be passed through the porphyrin solution. Partial CO pressures between 0.005 and 1 atm were obtained by using either pure CO or 10% CO–90% Ar mixtures as the source of carbon monoxide. Corrections were made for the vapor pressure of benzene.

NMR spectra were obtained on a Nicolet NT-300 spectrometer controlled by a Model 293-C pulse programmer and equipped with a 5-nm $^1H/^{13}C$ dual tuned probe or a General Electric QE-300 spectrometer. An IBM Model-100D electron spin resonance system was used to record ESR spectra. IR spectra were taken on an IBM Model 32 FTIR spectrophotometer.

Crystal Structure Determination. Single-crystal X-ray analyses of (OEP)Ir(C_3H_7)(PPh_3) and (OEP)Ir(C_3H_7)(Me_2SO) were performed at the University of Houston X-ray Crystallography Center. Final cell constants as well as other information pertinent to data collection and refinement are listed in Table I. For (OEP)Ir(C_3H_7)(PPh_3) a slight decay of 5.1% over the 102 h of exposure time was accounted for by a linear decay correction. In reduction of the data, Lorentz and polarization factors were applied, as well as an empirical absorption correction based on azimuthal ψ scans of six reflections having χ near 90°.[21] The structure was solved by interpretation of the Patterson map, which revealed the positions of the Ir and P atoms. The remaining non-hydrogen atoms were located in subsequent difference Fourier syntheses. A partial perdeuterated benzene of solvation was found and refined with all atoms at 50% occupancy factors. It is probably reasonable to assume that the solvent sites are initially fully occupied and that the volatile solvent slowly diffuses out of the crystal lattice, thus accounting for the observed decay. The usual sequence of isotropic and anisotropic refinement was followed, after which all hydrogens were entered in ideal calculated positions. After all shift/esd ratios were less than 0.5 (except for those associated with the C_6D_6), convergence was reached at the agreement factors listed in Table I. No unusually high correlations were noted between any of the variables in the last cycle of least-squares refinement, and the final difference density map showed no peaks greater than 1.00 e/Å^3. All calculations were made by using Molecular Structure Corp.'s TEXRAY 230 modifications of the SDP-PLUS series of programs.

The data for (OEP)Ir(C_3H_7)(Me_2SO) showed no decay. An empirical absorption correction based on 10 reflections was applied, and the structure was solved by use of the SHELXTL Patterson interpretation program. All hydrogens were entered in ideal calculated positions and constrained to riding motion, with a single variable isotropic temperature factor for all of them. Convergence was reached after all shift/esd ratios were less than 0.1, and no unusually high correlations were noted. The maximum residual density peak was about 2 e/Å^3, located quite close to the Ir atom. All calculations were made by using Nicolet's SHELXTL PLUS (1987) series of crystallographic programs.

Table I. Data Collection and Processing Parameters

	(OEP)Ir(C_3H_7)-(PPh_3) (1)	(OEP)Ir(C_3H_7)-(Me_2SO) (2)
space group	$P\bar{1}$	$P\bar{1}$
cell const		
a, Å	14.105 (7)	11.040 (5)
b, Å	14.098 (7)	11.179 (5)
c, Å	14.032 (8)	15.689 (7)
α, deg	89.20 (4)	95.58 (3)
β, deg	102.76 (4)	90.71 (3)
γ, deg	89.63 (4)	99.79 (3)
V, Å^3	2721	1898
mol formula	$C_{57}H_{66}N_4PIr \cdot {}^1/_2C_6D_6$	$C_{41}H_{57}N_4OSIr$
fw	1072.4	846.3
Z	2	2
ρ(calc), g/cm^3	1.31	1.48
μ, cm^{-1}	25.1	35.9
λ(Mo Kα), Å	0.710 73	0.710 73
$R(F_o)$	0.038	0.047
$R_w(F_o)$	0.051	0.046

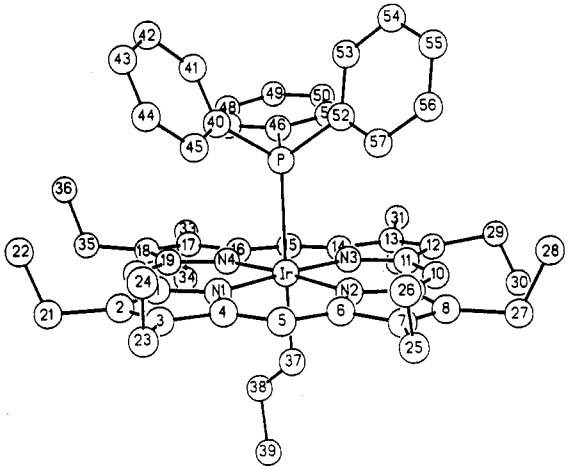

Figure 1. Molecular structure of (OEP)Ir(C_3H_7)(PPh_3), with hydrogens omitted for clarity.

Results and Discussion

Crystal Structures. The molecular structure of (OEP)Ir(C_3H_7)(PPh_3) (**1**) is presented in Figure 1 and that of (OEP)Ir(C_3H_7)(Me_2SO) (**2**) in Figure 2. Final atomic positional parameters are given in Table II, while Tables III and IV give selected bond distances and bond angles, respectively.

The iridium atom in **1** is in a fairly regular octahedral coordination environment, as expected for an iridium(III) hexacoordinated species. The phosphine ligand is bent about 6° away from N2, while the propyl ligand bends 6° toward N2. The

(20) Lin, X. Q.; Kadish, K. M. *Anal. Chem.* **1985**, *57*, 1498.
(21) North, A. C. T.; Phillips, D. C.; Matthews, F. S. *Acta Crystallogr., Sect. A: Cryst. Phys., Diffr., Theor. Gen. Crystallogr.* **1968**, *A24*, 351.

Table II. Positional Parameters and Their Estimated Standard Deviations[a]

A. (OEP)Ir(C_3H_7)(PPh_3)

atom	x	y	z	atom	x	y	z
Ir	0.34080 (3)	0.22829 (3)	0.21770 (3)	C30	0.402 (2)	0.353 (1)	0.657 (1)
P	0.1564 (2)	0.2299 (2)	0.1741 (2)	C31	0.305 (1)	0.543 (1)	0.462 (1)
N1	0.3512 (6)	0.1476 (5)	0.1008 (6)	C32	0.396 (2)	0.585 (1)	0.491 (1)
N2	0.3550 (6)	0.1099 (5)	0.3040 (6)	C33	0.323 (1)	0.6100 (8)	0.0852 (9)
N3	0.3376 (6)	0.3103 (5)	0.3355 (6)	C34	0.419 (1)	0.655 (1)	0.106 (1)
N4	0.3370 (6)	0.3490 (5)	0.1343 (6)	C35	0.319 (1)	0.4830 (8)	−0.1009 (9)
C1	0.3488 (8)	0.1807 (7)	0.0067 (7)	C36	0.219 (1)	0.483 (1)	−0.157 (1)
C2	0.3589 (9)	0.0994 (8)	−0.0524 (7)	C37	0.4905 (9)	0.2300 (8)	0.2580 (8)
C3	0.3665 (8)	0.0185 (7)	0.0037 (8)	C38	0.547 (1)	0.293 (1)	0.223 (1)
C4	0.3646 (7)	0.0505 (7)	0.1017 (7)	C39	0.658 (1)	0.287 (1)	0.259 (1)
C5	0.3716 (8)	−0.0072 (7)	0.1832 (8)	C40	0.0895 (8)	0.1909 (7)	0.0538 (8)
C6	0.3664 (7)	0.0202 (7)	0.2766 (7)	C41	0.0032 (9)	0.2338 (8)	0.0041 (9)
C7	0.3759 (8)	−0.0451 (7)	0.3593 (8)	C42	−0.052 (1)	0.197 (1)	−0.080 (1)
C8	0.3696 (8)	0.0082 (7)	0.4367 (8)	C43	−0.019 (1)	0.116 (1)	−0.1162 (9)
C9	0.3572 (7)	0.1065 (7)	0.4031 (7)	C44	0.065 (1)	0.0718 (9)	−0.0684 (9)
C10	0.3493 (9)	0.1830 (7)	0.4581 (7)	C45	0.1185 (9)	0.1099 (8)	0.0165 (9)
C11	0.3398 (9)	0.2779 (7)	0.4288 (7)	C46	0.1152 (8)	0.3516 (7)	0.1784 (8)
C12	0.331 (1)	0.3571 (8)	0.4896 (8)	C47	0.1126 (9)	0.4143 (7)	0.1017 (9)
C13	0.329 (1)	0.4353 (7)	0.4336 (8)	C48	0.090 (1)	0.5080 (9)	0.106 (1)
C14	0.3341 (8)	0.4073 (1)	0.3371 (7)	C49	0.070 (1)	0.5432 (9)	0.188 (1)
C15	0.3351 (8)	0.4664 (7)	0.2575 (8)	C50	0.074 (1)	0.4861 (9)	0.268 (1)
C16	0.3346 (8)	0.4401 (7)	0.1636 (7)	C51	0.0981 (9)	0.3872 (9)	0.2653 (9)
C17	0.3295 (8)	0.5048 (7)	0.0820 (8)	C52	0.0840 (8)	0.1645 (7)	0.2460 (8)
C18	0.3287 (8)	0.4517 (7)	0.0047 (8)	C53	−0.013 (1)	0.185 (1)	0.238 (1)
C19	0.3342 (8)	0.3530 (7)	0.0354 (7)	C54	−0.069 (1)	0.130 (1)	0.288 (1)
C20	0.3384 (8)	0.2749 (7)	−0.0216 (7)	C55	−0.0293 (9)	0.057 (1)	0.344 (1)
C21	0.364 (1)	0.1079 (9)	−0.161 (1)	C56	0.063 (1)	0.031 (1)	0.350 (1)
C22	0.267 (1)	0.115 (1)	−0.221 (1)	C57	0.1203 (9)	0.0861 (9)	0.297 (1)
C23	0.3741 (9)	−0.0817 (8)	−0.0251 (8)	C58	−0.015 (2)	0.762 (2)	0.356 (2)*
C24	0.279 (1)	−0.1322 (9)	−0.047 (1)	C59	−0.046 (2)	0.697 (2)	0.387 (2)*
C25	0.390 (1)	−0.1517 (8)	0.3557 (9)	C60	−0.029 (2)	0.636 (2)	0.470 (2)*
C26	0.297 (1)	−0.2023 (9)	0.313 (1)	C61	0.045 (2)	0.672 (2)	0.519 (2)*
C27	0.3755 (9)	−0.0255 (8)	0.5423 (8)	C62	0.092 (2)	0.717 (2)	0.487 (2)*
C28	0.278 (1)	−0.046 (1)	0.5626 (9)	C63	0.049 (2)	0.749 (2)	0.407 (2)*
C29	0.313 (1)	0.351 (1)	0.596 (1)				

B. (OEP)Ir(C_3H_7)(Me_2SO)

atom	10^4x	10^4y	10^4z	atom	10^4x	10^4y	10^4z
Ir	1721 (1)	3886 (1)	2597 (1)	C18	1129 (13)	7269 (10)	3927 (9)
S	754 (3)	4305 (3)	1279 (2)	C19	765 (12)	5971 (10)	3615 (9)
O	1484 (10)	4468 (12)	511 (7)	C20	−303 (11)	5211 (11)	3826 (8)
N1	57 (8)	3322 (8)	3077 (6)	C21	−2795 (12)	3724 (11)	4275 (9)
N2	1791 (9)	2147 (8)	2076 (6)	C22	−3626 (13)	4319 (14)	3782 (10)
N3	3406 (8)	4426 (9)	2137 (6)	C23	−2781 (11)	1017 (11)	3343 (8)
N4	1660 (9)	5611 (8)	3112 (6)	C24	−3567 (13)	825 (13)	2536 (10)
C1	−658 (11)	3991 (10)	3562 (7)	C25	482 (13)	−1148 (11)	1525 (11)
C2	−1801 (11)	3253 (11)	3765 (7)	C26	−536 (15)	−1241 (13)	891 (10)
C3	−1794 (11)	2123 (10)	3370 (7)	C27	3296 (14)	−282 (13)	947 (11)
C4	−634 (11)	2145 (10)	2967 (7)	C28	3175 (15)	−260 (14)	−5 (9)
C5	−242 (12)	1170 (10)	2507 (8)	C29	6351 (12)	3986 (13)	1088 (9)
C6	849 (11)	1155 (10)	2095 (8)	C30	6084 (14)	3669 (14)	118 (10)
C7	1266 (12)	101 (10)	1674 (8)	C31	6128 (13)	6833 (13)	1660 (10)
C8	2425 (12)	450 (11)	1411 (8)	C32	6962 (15)	7178 (14)	2439 (11)
C9	2754 (12)	1754 (10)	1672 (9)	C33	2931 (14)	8998 (12)	3552 (11)
C10	3837 (12)	2462 (11)	1529 (8)	C34	4010 (16)	9138 (14)	4125 (11)
C11	4140 (11)	3713 (12)	1717 (8)	C35	388 (13)	8026 (12)	4491 (10)
C12	5297 (12)	4457 (12)	1503 (9)	C36	−457 (14)	8649 (13)	4041 (9)
C13	5209 (12)	5634 (13)	1799 (8)	C37	2541 (12)	3610 (11)	3744 (9)
C14	4057 (13)	5626 (13)	2175 (9)	C38	2796 (18)	2477 (16)	3903 (10)
C15	3606 (13)	6613 (12)	2556 (10)	C39	3394 (15)	2462 (14)	4818 (10)
C16	2550 (13)	6620 (12)	3029 (11)	C40	−35 (16)	5509 (12)	1485 (10)
C17	2177 (14)	7670 (12)	3534 (9)	C41	−522 (11)	3189 (11)	953 (9)

[a] Starred values denote atoms refined isotropically.

average iridium–nitrogen distance is 2.039 ± 0.004 Å, which is similar to values reported for (OEP)Ir(C_8H_{13})[19] and for other non-porphyrin iridium complexes.[22,23] The iridium–phosphorus distance of 2.537 Å is significantly larger than the usually reported Ir–P distances of 2.248–2.452 Å.[24] Steric repulsions between the methyl group and the porphyrin macrocycle might be responsible for this lengthening, as might the presence of a trans σ bond to propane. Interactions between the porphyrin ring and PPh_3 are supported by the configuration of the PPh_3 group with respect to the porphyrin macrocycle. As shown in Figure 1, one of the phenyl rings is almost parallel to the porphyrin macrocycle. The Ir–P–C angles are 120.9 and 122.3° for Ph_1 and Ph_3, but

(22) Nord, G.; Mazell, A. C.; Mazell, R. G.; Farver, O. *Inorg. Chem.* **1983**, *22*, 3429.
(23) Cobbledick, R. E.; Einstein, F. W. B.; Farell, N.; Gilchrist, A. B.; Sutton, D. *J. Chem. Soc., Dalton Trans.* **1977**, 373.
(24) Churchill, M. R.; Bezman, S. A. *Inorg. Chem.* **1974**, *13*, 1418 and references 22–45 therein.

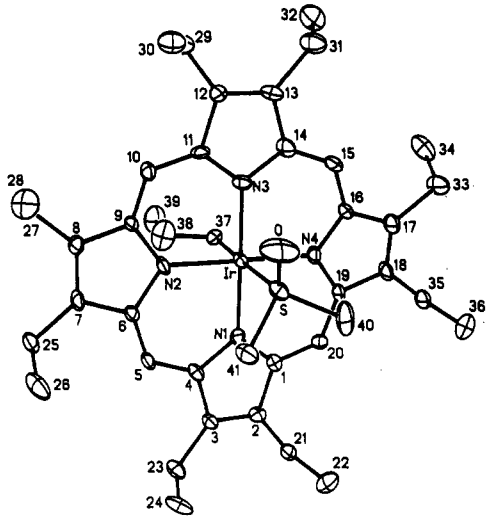

Figure 2. Molecular structure of (OEP)Ir(C_3H_7)(Me_2SO), with hydrogens omitted for clarity.

Table III. Selected Bond Distances (Å)[a]

	A. (OEP)Ir(C_3H_7)(PPh_3)		
Ir–P	2.537 (1)	C43–C44	1.372 (9)
Ir–N1	2.041 (4)	C44–C45	1.380 (8)
Ir–N2	2.030 (3)	C46–C47	1.377 (7)
Ir–N3	2.039 (4)	C46–C51	1.395 (7)
Ir–N4	2.045 (4)	C47–C48	1.364 (8)
Ir–C37	2.063 (6)	C48–C49	1.336 (10)
P–C40	1.836 (5)	C49–C50	1.371 (9)
P–C46	1.814 (5)	C50–C51	1.437 (8)
P–C52	1.831 (5)	C52–C53	1.372 (8)
C37–C38	1.354 (9)	C52–C57	1.343 (7)
C38–C39	1.527 (9)	C53–C54	1.399 (8)
C40–C41	1.393 (7)	C54–C55	1.340 (9)
C40–C45	1.360 (7)	C55–C56	1.333 (9)
C41–C42	1.372 (8)	C56–C57	1.438 (8)
C42–C43	1.364 (9)		
	B. (OEP)Ir(C_3H_7)(Me_2SO)		
Ir–S	2.436 (3)	S–O	1.47 (1)
Ir–N1	2.018 (9)	S–C40	1.73 (1)
Ir–N2	2.048 (8)	S–C41	1.75 (1)
Ir–N3	2.020 (9)	C37–C38	1.39 (1)
Ir–N4	2.029 (9)	C38–C39	1.58 (1)
Ir–C37	2.08 (1)		

[a] Numbers in parentheses are estimated standard deviations in the least significant digits.

108.1° is found for Ph_2. Concomitant differences are observed in the C–P–C angles, which are 103.4° for Ph_1/Ph_2, 103.0° for Ph_2/Ph_3, and 96.5° for Ph_1/Ph_3.

The iridium atom in (OEP)Ir(C_8H_{13}) is almost in the N_4 plane (Δ = 0.06 Å, toward P). The iridium–carbon bond distance is 2.063 Å and falls well within the range reported for other nonporphyrin Ir–carbon single-bonded complexes (1.97–2.19 Å).[25-29] However, a difference of 0.17 Å is observed in the Ir–carbon bond distances between (OEP)Ir(C_3H_7)(PPh_3) and (OEP)Ir(C_8H_{13}).[19] This difference reflects the fact that both the propyl group and the PPh_3 ligand compete for the same iridium orbital ($5d_{z^2}(6p_z,6s)$). On the other hand, one consequence is that the iridium atom is out of the plane toward phosphorus. This results in a larger electron repulsion with the π ring system, which tends to lengthen the Ir–carbon bond. All bond distances and angles of the octaethylporphyrin macrocycle are within the expected range.[19,30-32]

Table IV. Selected Bond Angles (deg)[a]

	A. (OEP)Ir(C_3H_7)(PPh_3)		
P–Ir–N1	93.3 (1)	Ir–P–C40	120.9 (2)
P–Ir–N2	95.9 (1)	Ir–P–C46	108.1 (2)
P–Ir–N3	89.5 (1)	Ir–P–C52	122.3 (2)
P–Ir–N4	88.1 (1)	C40–P–C46	103.0 (3)
P–Ir–C37	177.7 (2)	C40–P–C52	96.5 (2)
N1–Ir–N2	90.1 (2)	C46–P–C52	103.4 (3)
N1–Ir–N3	177.2 (2)	Ir–C37–C38	124.6 (5)
N1–Ir–N4	90.3 (2)	C37–C38–C39	119.3 (7)
N1–Ir–C37	89.0 (2)	P–C40–C41	122.8 (5)
N2–Ir–N3	90.2 (2)	P–C40–C45	118.9 (4)
N2–Ir–N4	175.9 (2)	P–C46–C47	121.6 (5)
N2–Ir–C37	84.0 (2)	P–C46–C51	119.9 (4)
N3–Ir–N4	89.1 (2)	P–C52–C53	121.3 (5)
N3–Ir–C37	88.3 (2)	P–C52–C57	120.4 (5)
N4–Ir–C37	91.9 (2)		
	B. (OEP)Ir(C_3H_7)(Me_2SO)		
S–Ir–N1	90.7 (3)	N3–Ir–N4	91.1 (4)
S–Ir–N2	90.3 (3)	N3–Ir–C37	89.4 (4)
S–Ir–N3	90.7 (3)	N4–Ir–C37	87.6 (4)
S–Ir–N4	89.8 (3)	Ir–S–O	119.9 (5)
S–Ir–C37	177.4 (4)	Ir–S–C40	110.0 (5)
N1–Ir–N2	90.8 (4)	Ir–S–C41	111.9 (5)
N1–Ir–N3	178.5 (4)	O–S–C40	110.0 (8)
N1–Ir–N4	89.4 (4)	O–S–C41	105.5 (7)
N1–Ir–C37	89.3 (4)	C40–S–C41	97.1 (7)
N2–Ir–N3	88.6 (4)	Ir–C37–C38	121.9 (10)
N2–Ir–N4	179.7 (2)	C37–C38–C39	113.7 (14)
N2–Ir–C37	92.3 (4)		

[a] Numbers in parentheses are estimated standard deviations in the least significant digits.

Table V. Electronic Absorption Spectral Data for (OEP)Ir(C_3H_7)(L) Complexes in Benzene

	λ_{max}, nm ($10^{-3}\epsilon$)				
ligand, L	Soret bands		Q-bands		
none	388 (185)		500 (15.3)	528 (45.8)	
py	346 (51)	399 (189)	504 (16.4)	533 (27.2)	
N-MeIm	344 (54)	403 (192)	504 (17.4)	532 (26.8)	
Me_2SO	359 (64)	402 (187)	513 (16.7)	539 (19.2)	
CO	356 (72)	408 (161)	525 (24.6)	502 (sh)	534 (15.1)
PPh_3	366 (85)	424 (87)	530 (14.3)	542 (14.1)	
$P(OEt)_3$	365 (118)	427 (71)	533 (18.1)		
NEt_3	345 (48)	400 (179)	504 (16.1)	634 (27.6)	

The iridium atom in **2** has a more regular octahedral environment than in **1**, with none of the N–Ir–S angles more than 0.7° away from 90°. The much smaller bulk of the Me_2SO is more easily accommodated in the axial position than PPh_3. The propane still bends away from one of the nitrogens (N2), but only by 2.5° in this case, and it appears from space-filling drawings that this may be due to some minor repulsion between the macrocycle π cloud and the hydrogens on C38. The average Ir–N distance is 2.029 (9) Å, essentially the same as in **1**. The Ir–S distance of 2.436 (3) Å is at the long end of the reported values in the literature and is considerably longer than the average 2.24 Å reported for other Ir–S bond lengths involving Me_2SO.[33,34] However, in one case the authors estimated the "normal" Ir–S distance to be 2.42 Å, based on analysis of covalent radii,[34] and this is in good agreement with our observation. The overall geometry of the Me_2SO moiety in the present case shows excellent agreement with literature values involving transition-metal complexes,[33-35] with the Ir–S–O angle (119.9°) much larger than that

(25) Bezman, S. A.; Bird, P. N.; Fraser, A. R.; Osborn, J. A. *Inorg. Chem.* **1980**, *19*, 3755.
(26) Shultz, A. J.; McArdle, J. V.; Khamore, G. P.; Eisenberg, R. *J. Organomet. Chem.* **1974**, *72*, 415.
(27) Thorn, D. L.; Tulip, T. H. *Organometallics* **1982**, *1*, 1580.
(28) Milstein, D.; Calabrese, J. C. *J. Am. Chem. Soc.* **1982**, *104*, 3773.
(29) Thorn, D. L.; Tulip, T. H. *J. Am. Chem. Soc.* **1981**, *103*, 5984.
(30) Takenaka, A.; Syal, S. K.; Sasada, Y.; Oruvra, T.; Ogaslie, H.; Yoshida, Z. *Acta Crystallogr., Sect. B: Struct. Crystallogr. Cryst. Chem.* **1976**, *32*, 62.
(31) Grigg, R. *Acta Crystallogr., Sect. B: Struct. Crystallogr. Cryst. Chem.* **1982**, *38*, 2455.
(32) Cullen, D. L.; Meyer, E. F.; Smith, K. M. *Inorg. Chem.* **1977**, *16*, 1179.
(33) Kisenyi, J. M.; Cabeza, J. A.; Smith, A. J.; Adams, H.; Sunley, G. J.; Salt, N. J. S.; Maitlis, P. M. *J. Chem. Soc., Chem. Commun.* **1985**, 770.
(34) McPartlin, M.; Mason, R. *J. Chem. Soc. A* **1970**, 2206.
(35) Bennet, M. J.; Cotton, F. A.; Weaver, D. L.; Williams, R. J.; Watson, W. H. *Acta Crystallogr.* **1967**, *23*, 788.

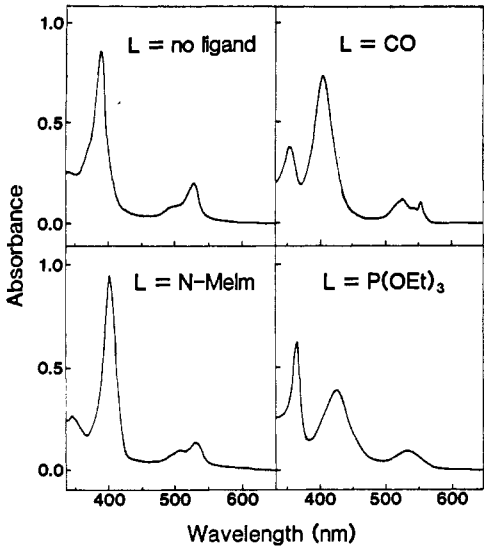

Figure 3. UV–visible spectra of (OEP)Ir(C_3H_7) and (OEP)Ir(C_3H_7)(L) in benzene, where L = CO, *N*-MeIm, and $P(OEt)_3$.

of Ir–S–C (average 111.0°) and the O–S–C angles (average 107.8°) much larger than that of C–S–C (97.1°).

The iridium atom is essentially in the N_4 plane (Δ = 0.01 Å, toward S), and the Ir–C bond distance of 2.08 Å is insignificantly different from the value found in **1**. The bonding geometry of the octaethylporphyrin is within normal values.[19,30-32]

Electronic Absorption Spectra of (OEP)Ir(C_3H_7) and (OEP)Ir(C_3H_7)(L) in Benzene. (OEP)Ir(C_3H_7) exhibits a typical UV–visible spectrum for a five-coordinate σ-bonded porphyrin complex.[36] The spectrum is also similar to UV–visible spectra reported for other (OEP)Ir(R) compounds,[17-19] and complexation with nitrogenous bases such as NEt_3, py, and *N*-MeIm leads to the expected red shift of each absorption band.[37]

The Soret band of (OEP)Ir(C_3H_7) is more affected by complexation than the Q-bands, and this is reflected by an additional band of variable intensity that is observed for (OEP)Ir(C_3H_7)(L) between 344 and 366 nm (see Table V and Figure 3). The formation of (OEP)Ir(C_3H_7)(L), where L = Me_2SO, CO, PPh_3, $P(OEt)_3$, yields a complex whose spectrum is characteristic of a hyperporphyrin.[36] The Soret band is split into two bands, which have maximum absorptions at 344–366 and 399–427 nm (see Table V). The hyper character of the spectrum is small for (OEP)Ir(C_3H_7)(Me_2SO), while (OEP)Ir(C_3H_7)($P(OEt)_3$) exhibits the highest hyper character as judged by the larger $\epsilon_{365}/\epsilon_{427}$ ratio.

Two types of metalloporphyrins, d and p, that exhibit hyper spectra have been identified on the basis of iterative extended Hückel (IEH) calculations.[38] The p types contain main-group metals in low oxidation states with $e_g(d_\pi)$ filled orbitals. In these cases, IEH shows that a metal to porphyrin charge-transfer transition is responsible for the split Soret band. The d type complexes include transition-metal porphyrins with vacancies in the $e_g(d_\pi)$ orbitals.[39] For these complexes, a charge transfer from the macrocycle ($a_{1u}(\pi)$, $a_{2u}(\pi)$ orbitals) to the metal ($e_g(d_\pi)$ orbital) leads to the split Soret band. This last type of hyperporphyrin spectrum best describes the (OEP)Ir(C_3H_7)(L) complexes. However, these types of charge-transfer transitions usually involve a change in metal oxidation state such as would be found for Ir(III) $\rightleftarrows$ Ir(II). In order for this transition to occur, the reduction potential for the Ir^{III}/Ir^{II} couple cannot be too negative.[39] This is not the case for the investigated complexes, as is discussed in later sections.

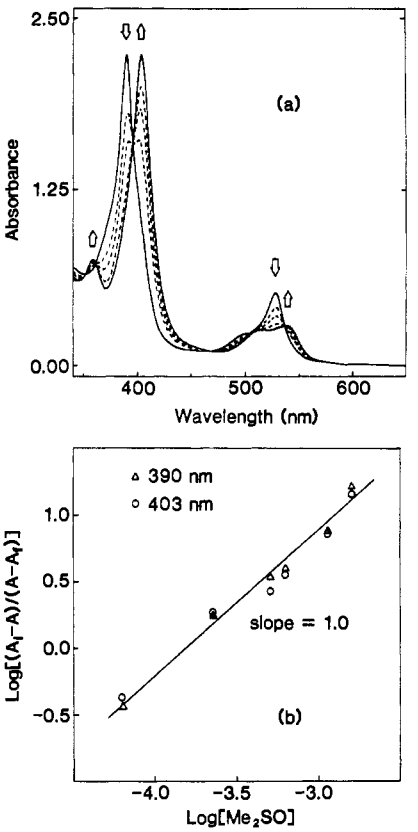

Figure 4. (a) UV–visible spectral changes observed during the titration of (OEP)Ir(C_3H_7) with Me_2SO in benzene. (b) log–log analysis of the spectral data.

Ligand-Addition Reactions of (OEP)Ir(C_3H_7) in Benzene. The ligand-binding reactions of (OEP)Ir(C_3H_7) with NEt_3, py, *N*-MeIm, Me_2SO, PPh_3, $P(OEt)_3$, and CO were monitored by UV–visible spectroscopy. These reactions were found to be fast and quantitative. Each isolated (OEP)Ir(C_3H_7)(L) complex was characterized by both UV–visible and ^1H NMR spectroscopy. The ligands utilized range from pure σ donor type ligands such as NEt_3 to π-acid donor type ligands such as CO.

Figure 4a shows the changes that occur in the electronic absorption spectra of (OEP)Ir(C_3H_7) during a titration with Me_2SO in benzene. Five-coordinate (OEP)Ir(C_3H_7) exhibits a Soret band at 388 nm and two Q-bands at 500 and 528 nm. The six-coordinate (OEP)Ir(C_3H_7)(Me_2SO) complex has a Soret band at 402 nm and two Q-bands at 513 and 539 nm. Four isosbestic points are obtained during the titration of (OEP)Ir(C_3H_7) with Me_2SO, indicating the presence of only two species in solution.

A log–log analysis of the spectral changes in Figure 4a was performed at 390 and 403 nm, and a plot of the data is shown in Figure 4b. The straight-line slope of 1.0 indicates the formation of a Me_2SO monoadduct according to eq 1, where L = Me_2SO.

$$\text{(OEP)Ir}(C_3H_7) + L \rightleftarrows \text{(OEP)Ir}(C_3H_7)(L) \qquad (1)$$

A stability constant of $K = 10^{3.8}$ was calculated from these data.

(OEP)Ir(C_3H_7) undergoes similar ligand-binding reactions with NEt_3 and py, and in both cases several isosbestic points were obtained during the titration. However, formation constants for binding of the other ligands were too large to determine spectrally by a direct titration with (OEP)Ir(C_3H_7). In these cases, indirect *K* values were obtained by monitoring the ligand-exchange reaction shown in eq 2, where L and L′ are one of seven different axial ligands.

$$\text{(OEP)Ir}(C_3H_7)(L) + L' \rightleftarrows \text{(OEP)Ir}(C_3H_7)(L') + L \qquad (2)$$

The same final UV–visible spectrum of a given six-coordinate complex could be obtained by starting either from five-coordinate (OEP)Ir(C_3H_7) or six-coordinate (OEP)Ir(C_3H_7)(L). For example, the addition of *N*-MeIm to either (OEP)Ir(C_3H_7) or

(36) Gouterman, M. In *The Porphyrins*; Dolphin, D., Ed.; Academic Press: New York, 1978; Vol. III.
(37) Cornillon, J.-L.; Anderson, J. E.; Kadish, K. M. *Inorg. Chem.* **1986**, *25*, 991 and references therein.
(38) Buchler, J. W. In *Porphyrins and Metalloporphyrins*; Smith, K. M., Ed.; Elsevier: Amsterdam, 1975; Chapter 5.
(39) Gouterman, M.; Hanson, L. K.; Khalil, G.-E.; Lecustre, W. R.; Buchler, J. W. *J. Chem. Phys.* **1975**, *62*, 2343.

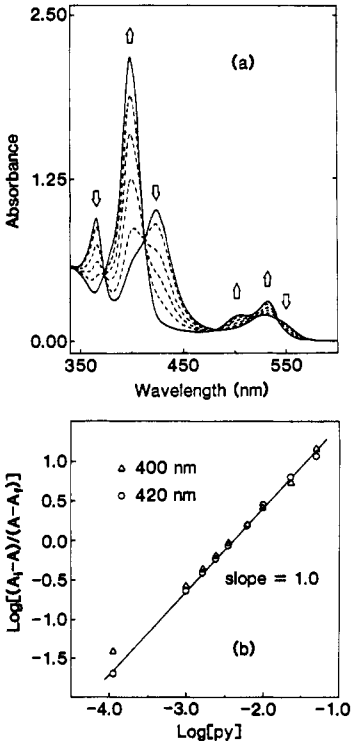

Figure 5. (a) UV–visible spectral changes observed during the titration of (OEP)Ir(C_3H_7)(PPh_3) by py in a benzene solution containing 0.01 M PPh_3. (b) log–log analysis of the spectral data.

Table VI. Stability Constants for the Formation of (OEP)Ir(C_3H_7)(L) from (OEP)Ir(C_3H_7)

ligand	log K	ligand	log K
py	4.8 ± 0.4	PPh_3	6.1 ± 0.4
N-MeIm	5.6 ± 0.4	$P(OEt)_3$	8.2 ± 0.8
Me_2SO	3.8 ± 0.4	NEt_3	1.6 ± 0.1
CO	5.0 ± 0.4		

(OEP)Ir(C_3H_7)(PPh_3) gave the same spectrum of (OEP)Ir(C_3H_7)(*N*-MeIm).

An example of the reaction in eq 2 is given by the data in Figure 5, which illustrates changes in the electronic absorption spectra of (OEP)Ir(C_3H_7)(PPh_3) in benzene containing 10^{-2} M PPh_3 and various concentrations of pyridine. The (OEP)Ir(C_3H_7)(PPh_3) complex exhibits a split Soret band at 366 and 424 nm and two Q-bands at 530 and 542 nm, while (OEP)Ir(C_3H_7)(py) has a Soret band at 399 nm and two Q-bands at 504 and 533 nm. Four isosbestic points at 374, 414, 484, and 543 nm are observed during the titration of (OEP)Ir(C_3H_7)(PPh_3) in benzene, 10^{-2} M PPh_3 with pyridine. Log–log analysis of the spectral changes are shown in Figure 5b and yield a straight line with a slope of 1.0.

With use of the experimentally determined value of K_1 for pyridine addition, a calculated value of $K = 10^{6.1}$ was estimated for PPh_3 addition according to eq 1. Titrations of (OEP)Ir(C_3H_7)(L) with the other ligands enabled the calculation of stability constants for the formation of (OEP)Ir(C_3H_7)(L) complexes. These values are summarized in Table VI.

^{1}H NMR Spectra of (OEP)Ir(C_3H_7)(L) in Benzene-d_6. (OEP)Ir(C_3H_7) exhibits the normal octaethylporphyrin ^{1}H NMR resonances in C_6D_6.[40] The meso proton resonances are at 9.92 ppm, while the ethyl groups have CH_2 and CH_3 resonances at 3.92 and 1.90 ppm, respectively. The propyl protons are shifted upfield by up to 7 ppm, as expected for an alkyl group attached to the central metal ion. This is due to the well-known large diamagnetic ring current of the porphyrin ring.[18] The resonances at −5.70 ppm (triplet), −4.51 ppm (multiplet), and −2.05 ppm (triplet) can be unambiguously assigned as the α-CH_2, β-CH_2, and γ-CH_3 resonances of the propyl group σ-bonded to the iridium atom.

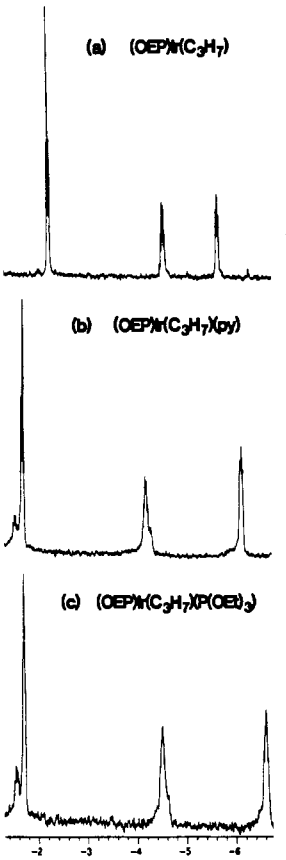

Figure 6. High-field region of the ^{1}H NMR spectrum of (a) (OEP)Ir(C_3H_7), (b) (OEP)Ir(C_3H_7)(py), and (c) (OEP)Ir(C_3H_7)($P(OEt)_3$) in C_6D_6.

Table VII. ^{1}H NMR Data for the (OEP)Ir(C_3H_7)(L) Complexes in Benzene-d_6[a]

	OEP protons			C_3H_7 protons		
ligand, L	meso	α-CH_2	β-CH_3	α-CH_2	β-CH_2	γ-CH_3
none	9.92	3.92	1.90	−5.70	−4.51	−2.05
py	9.95	3.91	1.89	−6.12	−4.18	−1.67
N-MeIm	9.91	3.94	1.91	−6.18	−4.03	−1.62
Me_2SO	10.03	3.93	1.87	−6.03	−4.43	−1.84
CO	10.24	3.95	1.88	−6.57	−4.70	−1.86
PPh_3	9.91	3.86	1.86	−6.62[b]	−4.68	−1.86
$P(OEt)_3$	9.99	3.94	1.90	−6.60[b]	−4.51	−1.68
NEt_3	9.95	3.93	1.90	−5.70	−4.48	−2.02

[a] Values good to ±0.01 ppm. [b] Coupling from P observed: 14 Hz for PPh_3; 17 Hz for $P(OEt)_3$.

Bonding of a sixth axial ligand to (OEP)Ir(C_3H_7) causes dramatic shifts of the propyl proton resonances. This is shown in Figure 6, while Table VII summarizes ^{1}H NMR data for (OEP)Ir(C_3H_7) and the seven different (OEP)Ir(C_3H_7)(L) complexes. Complexation of (OEP)Ir(C_3H_7) with a sixth axial ligand causes the α-CH_2 resonances to shift upfield 0.00–0.92 ppm and the γ-CH_3 resonances to shift downfield by 0.03–0.43 ppm (see Figure 6a,b and Table VII). However, the specific chemical shifts of the β-CH_2 protons depend upon the nature of the ligands coordinated to the iridium atom.

It is of particular interest to note that only complexes with bound CO and PPh_3 have β-CH_2 upfield shifts, and this may be attributed to the strong π-back-bonding properties of these two groups. A P–$H_{\alpha\text{-}CH_2}$ coupling of 17 Hz is observed for (OEP)Ir(C_3H_7)($P(OEt)_3$) (see Figure 6c), indicating a competition between the P and C atoms for the same valence orbitals ($5d_{z^2}$($6p_z$,6s)) of the iridium atom. This contributes to the efficient transmission of coupling effects between the nuclei of the two trans-coordinated ligands.

(40) Janson, T. R.; Katz, J. J. In *The Porphyrins*; Dolphin, D., Ed.; Academic Press: New York, 1978; Vol. IV.

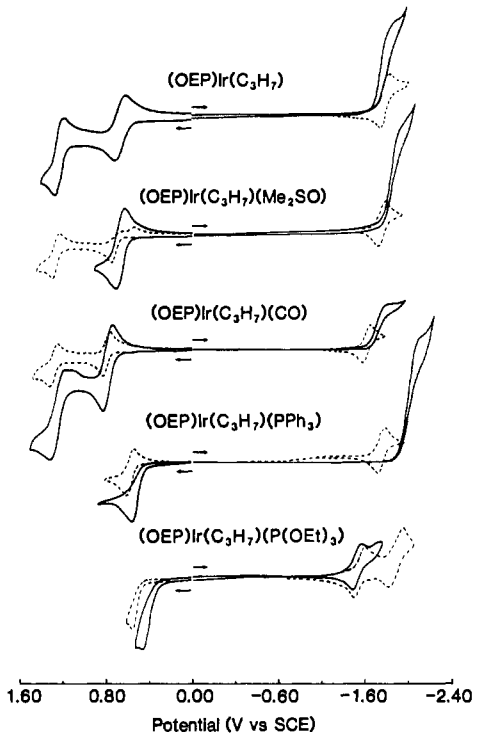

Figure 7. Cyclic voltammograms of (OEP)Ir(C_3H_7) and (OEP)Ir(C_3H_7)(L) in CH_2Cl_2, 0.1 M (TBA)ClO_4 at room temperature (—) and at −77 °C (---) (scan rate 100 mV/s).

The ^1H NMR resonances of (OEP)Ir(C_3H_7)(L) depend upon both the electron density at the metal center and the relative displacement of the central Ir atom from the porphyrin plane. The closer the propyl group is to the porphyrin plane, the more interaction there will be with the porphyrin π ring system and the more shielded will be the protons. For example, the iridium atom of (OEP)Ir(C_3H_7)(PPh_3) is slightly out of the porphyrin plane toward P (see Crystal Structures). As a consequence, both the α-CH_2 and the β-CH_2 protons are closer to the π ring system and are thus more shielded than in the case of (OEP)Ir(C_3H_7).

The electronic and steric repulsions between the propyl group and the porphyrin plane also result in a deshielding of the γ-CH_3 protons. In addition, the bonding of PPh_3 or $P(OEt)_3$ to (OEP)Ir(C_3H_7) results in more electron density being transferred to the iridium atom, so that the α-CH_2 protons are more electronegative in these complexes than in (OEP)Ir(C_3H_7). This also increases the shielding of the α-CH_2 protons.

The meso protons of octaethylporphyrins are extremely sensitive to changes of electron density on the macrocycle.[40] The more electron density transferred to the metal of (OEP)MX (by changing X^-), the more upfield the meso protons will be shifted.[22] This has been illustrated for a series of (OEP)In(R) complexes,[41] which show good agreement between the electron-donating ability of the R group and the shift of the meso protons. However, the influence of axial ligands on the chemical shifts of the meso protons is not as large as those on the propyl protons. A total difference ranging from 0.01 to 0.32 ppm is obtained. Almost no shift or small downfield shifts were observed for all but one of the (OEP)Ir(C_3H_7)(L) complexes compared to the signals for (OEP)Ir(C_3H_7). The only exception was (OEP)Ir(C_3H_7)(CO), as seen in Table VII. The relatively large downfield shifts for this complex reflect a lower electron density on the iridium–porphyrin π ring system and are due to the presence of π back-bonding into the CO orbitals.

Electrochemistry of (OEP)Ir(C_3H_7)(L). Cyclic voltammograms of (OEP)Ir(C_3H_7) and four (OEP)Ir(C_3H_7)(L) complexes in CH_2Cl_2, 0.1 M (TBA)ClO_4 are illustrated in Figure 7. (OEP)Ir(C_3H_7) undergoes two reversible room-temperature oxidations at $E_{1/2}$ = 0.65 and 1.23 V and one irreversible room-temperature reduction at E_{pc} = −1.88 V (scan rate 0.2 V/s) in CH_2Cl_2. The reduction becomes reversible at low temperature (see dashed line in Figure 7) or at scan rates greater than 1 V/s.

Table VIII. Half-Wave Potentials (V) for the Oxidation and Reduction of (OEP)Ir(C_3H_7) and (OEP)Ir(C_3H_7)(L) in CH_2Cl_2, 0.1 M (TBA)ClO_4[a]

	oxidn[c]		1st redn	
ligand, L (concn)[b]	2nd	1st	25 °C	−77 °C
none	1.23	0.65	−1.88[d]	−1.77
Me_2SO (0.01 M)	1.26[e]	0.66	~−1.9[d]	−1.74
CO (1 atm)	1.27[e]	0.78	−1.80[d]	−1.60
PPh_3 (0.01 M)		0.57[e]		−1.93
$P(OEt)_3$ (0.01 M)		0.43[f]	−1.53	−1.54[g]
py (0.01 M)		0.55		−1.87
N-MeIm (0.1 M)		0.47		−1.95

[a] The concentration of (OEP)Ir(C_3H_7) ranged between 1.3×10^{-3} and 2.0×10^{-3} M. [b] Concentration of ligand in CH_2Cl_2 solutions. [c] Values of $E_{1/2}$ at 25 °C unless otherwise indicated. [d] E_{pc} at a scan rate of 0.2 V/s. [e] At −77 °C. [f] E_{pa} at a scan rate of 0.1 V/s. [g] A second reversible low-temperature (−77 °C) reduction is observed at −1.86 V as illustrated in Figure 7.

(OEP)Ir(C_3H_7)(Me_2SO) exhibits a reversible one-electron room-temperature oxidation at $E_{1/2}$ = 0.66 V and an irreversible one-electron reduction at $E_p \approx -1.9$ V. The cyclic voltammograms of (OEP)Ir(C_3H_7) and (OEP)Ir(C_3H_7)(Me_2SO) are similar at room temperature, but this is not the case at −77 °C, where the first oxidation peak of (OEP)Ir(C_3H_7)(Me_2SO) is coupled to two re-reduction peaks as shown by the dashed line in Figure 7. A similar voltammogram also occurs at room temperature when scan rates greater than 1.0 V/s are employed.

The exact mechanism for the oxidation of (OEP)Ir(C_3H_7)(Me_2SO) in CH_2Cl_2–Me_2SO mixtures is not known. However, a rate-determining dissociation of Me_2SO from electrochemically generated [(OEP)Ir(C_3H_7)(Me_2SO)]$^+$ can be ruled out by the constancy of $E_{1/2}$ in various mixtures of CH_2Cl_2 and Me_2SO. No shift in $E_{1/2}$ occurs in CH_2Cl_2 containing Me_2SO at concentrations between 5×10^{-4} and 1.0 M, and this clearly suggests that Me_2SO does not dissociate upon oxidation during the time scale of the electrochemical experiment.

One possible explanation for the oxidative behavior of (OEP)Ir(C_3H_7)(Me_2SO) at low temperature might be that the Me_2SO mode of binding changes with a change in the porphyrin oxidation state, as has been reported to occur for $Rh_2(ac)_4(Me_2SO)_2$.[42] Me_2SO is proposed to bind to $Rh_2(ac)_4$ via S in the neutral form and via O upon formation of $[Rh_2(ac)_4]^+$. A change of the Me_2SO linkage upon formation of [(OEP)Ir(C_3H_7)(Me_2SO)]$^+$ might be slowed down sufficiently at low temperature and/or fast scan rates so that two forms of the Me_2SO complex (S bonded and O bonded) might be reduced on the reverse scan. In this case, two oxidation peaks might be observed. However, no additional evidence for this suggested mechanism is available.

(OEP)Ir(C_3H_7)(CO) exhibits two oxidations and a single reduction in CH_2Cl_2 under 1 atm of CO (see Figure 7). The first oxidation is reversible and occurs at $E_{1/2}$ = 0.78 V. The second oxidation is quasireversible at room temperature but reversible at low temperature. The first reduction of (OEP)Ir(C_3H_7)(CO) is irreversible at room temperature but also becomes reversible at −77 °C. Values of $E_{1/2}$ for these reactions are summarized in Table VIII.

The partial pressure of CO over CH_2Cl_2 solutions of (OEP)Ir(C_3H_7) was changed from 0.1 to 1.0 atm, and a 15-mV shift in $E_{1/2}$ was observed. This shift compares to a theoretical value of 59 mV for the loss of one CO from the oxidized species and suggests that no loss of CO occurs upon electrooxidation.

(OEP)Ir(C_3H_7)(PPh_3) undergoes only one oxidation and one reduction within the solvent potential window of CH_2Cl_2 containing

(41) Cocolios, P.; Guilard, R.; Fournari, R. *J. Organomet. Chem.* **1979**, *179*, 311.

(42) Chavan, M. Y.; Lin, X. Q.; Bernal, I.; Bear, J. L.; Kadish, K. M. *Inorg. Chem.* **1986**, *25*, 1281.

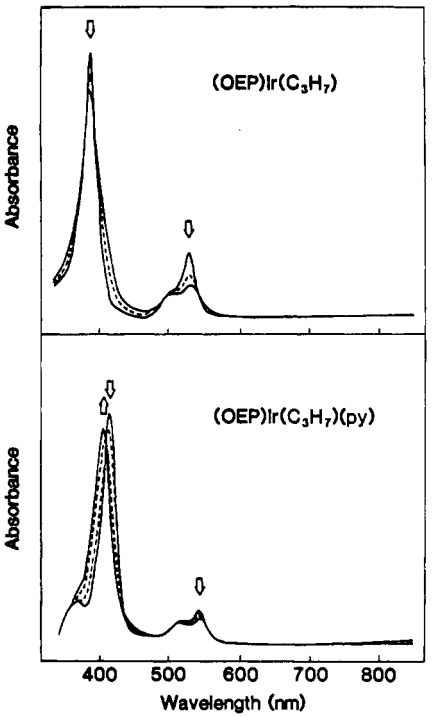

Figure 8. UV–visible spectral changes observed during the first oxidation of (OEP)Ir(C_3H_7) and (OEP)Ir(C_3H_7)(py) in CH_2Cl_2, 0.1 M (TBA)ClO_4.

0.01 M PPh_3 (which has an oxidation limit of +1.0 V vs SCE). Both reactions are irreversible at room temperature but are reversible at −77 °C (see dashed line in Figure 7). At this latter temperature, the value of $E_{1/2}$ for oxidation of the complex is independent of scan rate. However, at room temperature, the peak potential for the first oxidation is shifted by 33 mV for each 10-fold increase in scan rate, thus suggesting that this one-electron abstraction is followed by a fast chemical reaction (an electrochemical EC mechanism).

Unlike (OEP)Ir(C_3H_7)(PPh_3), (OEP)Ir(C_3H_7)($P(OEt)_3$) undergoes one irreversible oxidation and one reversible reduction at room temperature. The first oxidation remains irreversible even at low temperature. The single room-temperature reduction of (OEP)Ir(C_3H_7)($P(OEt)_3$) occurs at $E_{1/2}$ = −1.53 V, but a second reversible reduction at $E_{1/2}$ = −1.86 V is observed at −77 °C. Blank experiments demonstrate that free $P(OEt)_3$ is not oxidized or reduced within the potential range of the solvent, and this suggests that two electrons may be added in two steps to (OEP)Ir($P(OEt)_3$) at low temperature.

The behavior of (OEP)Ir(C_3H_7)(py) and (OEP)In(C_3H_7)(*N*-MeIm) is similar to that of the other (OEP)Ir(C_3H_7)(L) complexes in that the reductions are only reversible at −77 °C. The first oxidation of both (OEP)Ir(C_3H_7)(*N*-MeIm) and (OEP)Ir(C_3H_7)(py) occurs at a more negative potential than for oxidation of (OEP)Ir(C_3H_7). In addition, the low-temperature reduction of the *N*-MeIm and py complexes occurs at $E_{1/2}$ values that are more negative than for reduction of the five-coordinate species. The addition of a sixth axial ligand to generate (OEP)Ir(C_3H_7)(L) leads to complexes that are easier to oxidize in all cases except when L = CO. The strong π back-bonding of CO may contribute to this one exception by lowering the electron density either on the metal or on the π-ring system.

Spectroelectrochemistry of (OEP)Ir(C_3H_7)(L). The UV–visible spectroelectrochemistry of (OEP)Ir(C_3H_7)(L) was investigated in CH_2Cl_2, 0.1 M (TBA)ClO_4. Figure 8 shows the spectral changes observed during oxidation of (OEP)Ir(C_3H_7). The neutral species exhibits a Soret band at 388 nm and two Q bands at 500 and 529 nm. The Soret band blue-shifts upon oxidation and slightly decreases in intensity. At the same time, two new absorption bands appear at 503 and 531 nm. Isosbestic points are observed at 394, 494, and 540 nm, and the original spectrum can be recovered upon back-reduction. The observed UV–visible changes are not typical for formation of a porphyrin cation radical and do not support the formulation of a π-cation radical as the first oxidation product of (OEP)Ir(C_3H_7). The reversibility obtained on the thin-layer cyclic voltammetric time scale (2 mV/s) indicates that there is no cleavage of the Ir–carbon bond upon oxidation and is consistent with a strong Ir–C bond. (See Crystal Structures and Ligand-Addition Reactions.)

Table IX. Electronic Absorption Spectral Data for (OEP)Ir(C_3H_7)(L) and the First Oxidation Product in CH_2Cl_2, 0.1 M (TBA)ClO_4

ligand	electrode reacn	λ_{max}, nm ($10^{-3}\epsilon$) Soret bands		Q-bands	
none	none	388 (174)		500 (18.3)	529 (37.9)
	1st oxidn	384 (154)		504 (13.1)	531 (16.5)
py	none	399 (187)		506 (21.5)	532 (31.0)
	1st oxidn	389 (167)		500 (20.4)	532 (23.1)
N-MeIm	none	400 (196)		505 (20.4)	532 (29.6)
	1st oxidn	390 (177)		507 (20.3)	534 (23.1)
Me_2SO	none	402 (175)		513 (19.9)	539 (22.4)
	1st oxidn	386 (187)		502 (16.5)	531 (22.4)
CO	none	360 (70)	408 (154)	526 (23.8)	534 (15.4)
	1st oxidn[a]	394 (189)		513 (13.4)	545 (27.3)
PPh_3	none	367 (86)	423 (90)	530 (19.2)	547 (sh)
	1st oxidn[b]	397 (139)		512 (21.4)	545 (25.8)
$P(OEt)_3$	none	365 (119)	427 (73)	533 (18.4)	547 (sh)
	1st oxidn[c]	408 (140)		520 (22.4)	550 (27.2)

[a] The initial product was not stable upon oxidation, and the final spectral product is identified as (OEP)Ir(CO)ClO_4. [b] Product identified as (OEP)Ir(PPh_3)ClO_4; sh = shoulder. [c] Product identified as (OEP)Ir($P(OEt)_3$)ClO_4 (see text).

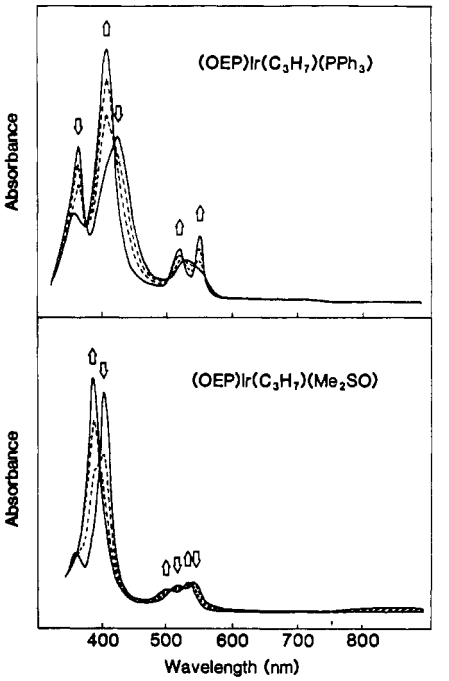

Figure 9. UV–visible spectral changes observed during the first oxidation of (OEP)Ir(C_3H_7)(PPh_3) and (OEP)Ir(C_3H_7)(Me_2SO) in CH_2Cl_2, 0.1 M (TBA)ClO_4.

Similar spectral changes are obtained upon oxidation of (OEP)Ir(C_3H_7)(py) (Figure 8) and (OEP)Ir(C_3H_7)(Me_2SO) (Figure 9). Table IX summarizes the spectral data of the neutral and six singly oxidized (OEP)Ir(C_3H_7)(L) complexes in CH_2Cl_2, 0.1 M (TBA)ClO_4.

The first oxidation product of (OEP)Ir(C_3H_7)(CO) is not stable under the conditions required for thin-layer spectroelectrochemistry, and a controlled-potential reduction does not regenerate the original spectrum. The voltammetric results under a CO atmosphere and the spectroelectrochemistry results for the first oxi-

dation of $(OEP)Ir(C_3H_7)(CO)$ indicate that $(OEP)Ir(CO)ClO_4$ is the singly oxidized product. A similar spectral result is obtained during oxidation of $(OEP)Ir(C_8H_{13})(CO)$ and leads to the formation of $(OEP)Ir(CO)ClO_4$.[19]

The cyclic voltammograms for oxidation of $(OEP)Ir(C_3H_7)(PPh_3)$ and $(OEP)Ir(C_3H_7)(P(OEt)_3)$ are irreversible, and this is consistent with the irreversible spectral changes obtained upon oxidation of the complexes in a thin-layer cell. The resulting spectral changes during oxidation of $(OEP)Ir(C_3H_7)(PPh_3)$ are illustrated in Figure 9. The original six-coordinate porphyrin exhibits a split Soret band at 367 and 423 nm and two Q bands at 530 and 547 nm. A new Soret band appears at 397 nm, and two well-defined Q bands appear at 512 and 545 nm after oxidation at 0.70 V. Six isosbestic points are obtained during oxidation, but these changes were not reversible and no spectral changes were monitored during the reverse controlled-potential reduction at 0.0 V.

Infrared spectroelectrochemistry was used in order to ascertain the final site of the electron transfer in $(OEP)Ir(C_3H_7)$ and $(OEP)Ir(C_3H_7)(L)$, where L = py, *N*-MeIm, or Me_2SO. Cation radicals of octaethylporphyrins[43] have been characterized as having a diagnostic absorption band between 1570 and 1520 cm^{-1}, but infrared spectra recorded after the one-electron oxidation of $(OEP)Ir(C_3H_7)$ and $(OEP)Ir(C_3H_7)(Me_2SO)$ do not show any absorptions between 1620 and 1480 cm^{-1}. This agrees with the UV-visible results and suggests that the site of the electron abstraction may not be at the porphyrin π ring system.

Finally, the products of controlled-potential oxidation were also monitored by ESR spectroscopy. Complete electrolysis required 1.0 ± 0.1 electrons for oxidation of each $(OEP)Ir(C_3H_7)(L)$ complex. When a sixth ligand was not bound to $(OEP)Ir(C_3H_7)$ or when L was py, *N*-MeIm, or Me_2SO, the oxidized product, $[(OEP)Ir(C_3H_7)]^+$ or $[(OEP)Ir(C_3H_7)(L)]^+$, exhibited an ESR signal centered at $g = 2.00$ with a peak-to-peak separation between 15 and 40 G.

Acknowledgment. The support of the National Science Foundation (Grant CHE-8515411) is gratefully acknowledged. We also acknowledge discussions with Dr. P. F. Blanchet.

Registry No. **1**, 120086-16-0; **2**, 120120-20-9; $(OEP)Ir(C_3H_7)$, 120086-15-9; $(OEP)Ir(C_3H_7)(py)$, 120086-17-1; $(OEP)Ir(C_3H_7)$(*N*-MeIm), 120086-18-2; $(OEP)Ir(C_3H_7)(CO)$, 120086-19-3; $(OEP)Ir(C_3H_7)(P(OEt)_3)$, 120086-20-6; $(OEP)Ir(C_3H_7)(NEt_3)$, 120086-21-7; (OEP)Ir(CO)Cl, 68324-58-3; $CH_3(CH_2)_2I$, 107-08-4.

Supplementary Material Available: Tables of hydrogen atomic coordinates, anisotropic thermal parameters, and all intramolecular distances and angles (15 pages); listings of observed and calculated structure factors (60 pages). Ordering information is given on any current masthead page.

(43) Shimonmura, E. T.; Phillippi, M. A.; Goff, H. M. *J. Am. Chem. Soc.* **1981**, *103*, 6778.

Contribution from the Department of Chemistry, University of Houston, Houston, Texas 77204-5641, Laboratoire de Chimie Physique Générale, Faculté des Sciences de Rabat, Université Mohammed V, Rabat, Morocco, and Laboratoire de Synthèse et d'Electrosynthèse Organométallique, Associé au CNRS (UA 33), Faculté des Sciences "Gabriel", Université de Dijon, 21100 Dijon, France

Electrochemistry of Nickel "Picket Fence" Porphyrin. Electrogeneration and Spectral Characterization of Nickel Complexes in Unusual Oxidation States

K. M. Kadish,*[1a] D. Sazou,[1a] G. B. Maiya,[1a] B. C. Han,[1a] Y. M. Liu,[1a] A. Saoiabi,[1b] M. Ferhat,[1b] and R. Guilard*[1c]

Received November 30, 1988

The electrochemical and spectroelectrochemical characterization of nickel(II) *meso*-α,α,α,α-tetrakis(*o*-pivalamidophenyl)porphyrin, (TpivPP)Ni, in dichloromethane, benzonitrile, and tetrahydrofuran is reported. The oxidative behavior of this complex is different from that of all previously studied nickel porphyrins. The complex is reversibly oxidized by three electrons in two steps and generates as a final product $[(TpivPP)Ni]^{3+}$, which was characterized as a Ni(IV) cation radical in solution by both UV-visible and ESR spectroscopy. The electroreduction of (TpivPP)Ni involves a stepwise addition of two electrons to the porphyrin π ring system. The electrogenerated $[(TpivPP)Ni]^-$ was characterized by UV-visible and ESR spectroscopy in THF and was shown to catalyze the electrochemical reduction of methyl iodide.

Introduction

The electrochemistry of "picket fence", "basket handle", and binary "face to face" porphyrins has been reported.[2-8] These compounds are structurally similar in that they all have amide- or ether-linked chains attached to the ortho position of the four phenyl groups of a tetraphenylporphyrin macrocycle. Most electrochemical studies of these compounds involved characterization of iron[2,4-6] and cobalt[7] derivatives, and studies on the electron-transfer reactivity of related porphyrins with other central metals are sparse.[3,8] It has been shown that the "picket fence" porphyrin (TpivPP)Cu, where TpivPP is the dianion of *meso*-α,α,α,α-tetrakis(*o*-pivalamidophenyl)porphyrin, as well as amide-linked "basket handle" porphyrins of Cu, Zn, and Mg undergo a reversible overall two-electron oxidation in nonaqueous media.[3] No other "picket fence" porphyrins have been investigated with respect to their oxidative behavior, nor has the reductive behavior of any metalated "superstructured" porphyrin containing other than iron or cobalt been reported.[9]

This present study reports the synthesis and electrochemistry of (TpivPP)Ni in CH_2Cl_2, PhCN, and THF. This complex, whose structure is shown in Figure 1, is of special interest in under-

(1) (a) University of Houston. (b) Université Mohammed V. (c) Université de Dijon.
(2) Lexa, D.; Momenteau, M.; Rentien, P.; Rytz, G.; Savéant, J.-M.; Xu, F. *J. Am. Chem. Soc.* **1984**, *106*, 4755.
(3) Lexa, D.; Maillard, P.; Momenteau, M.; Savéant, J.-M. *J. Am. Chem. Soc.* **1984**, *106*, 6321.
(4) Lexa, D.; Momenteau, M.; Savéant, J.-M.; Xu, F. *Inorg. Chem.* **1985**, *24*, 122.
(5) Lexa, D.; Momenteau, M.; Savéant, J.-M.; Xu, F. *J. Am. Chem. Soc.* **1986**, *108*, 6937.
(6) Gueutin, C.; Lexa, D.; Momenteau, M.; Savéant, J.-M.; Xu, F. *Inorg. Chem.* **1986**, *25*, 4294.
(7) Collman, J. P.; Marrocco, M.; Elliott, C. M.; L'Her, M. *J. Electroanal. Chem. Interfacial Electrochem.* **1981**, *124*, 113.
(8) Becker, J. Y.; Dolphin, D.; Paine, J. B.; Wijesekera, T. *J. Electroanal. Chem. Interfacial Electrochem.* **1984**, *164*, 335.

(9) The electrochemical reduction of the free base porphyrin, $(TpivPP)H_2$, was investigated in DMF by: Bump, C. M. Ph.D. Dissertation, The Pennsylvania State University, 1979. $(TpivPP)H_2$ is reduced via two successive one-electron transfers, and the overall reduction follows an ECEC mechanism. The first chemical step was assigned to a conformational change of the complex and the second step to a protonation reaction that resulted from trace H_2O in the DMF and led to the formation of a phlorin, the final electroreduction product.

0020-1669/89/1328-2542$01.50/0